Bound Hole States Associated to Individual Vanadium Atoms Incorporated into Monolayer WSe 2

Pierre Mallet, Florian Chiapello, Hanako Okuno, Hervé Boukari, Matthieu Jamet, Jean-Yves Veuillen

HAL Id: hal-02928456
https://hal.science/hal-02928456

Submitted on 6 Oct 2020

Bound hole states associated to individual vanadium atoms incorporated into monolayer WSe$_2$

Pierre Mallet,[1, 2, *] Florian Chiapello,[1, 2] Hanako Okuno,[3]
Hervé Boukari,[1, 2] Matthieu Jamet,[4] and Jean-Yves Veuillen[1, 2]

[1]*Université Grenoble Alpes, Institut Neel, F-38042 Grenoble, France*
[2]*CNRS, Institut Neel, F-38042 Grenoble, France*
[3]*Université Grenoble Alpes, CEA, IRIG-MEM, 38000 Grenoble, France*
[4]*Université Grenoble Alpes, CEA, CNRS, Grenoble INP, IRIG-SPINTEC, 38000 Grenoble, France*
(Dated: June 10, 2020)

Doping a two-dimensional semiconductor with magnetic atoms is a possible route to induce magnetism in the material. We report on the atomic structure and electronic properties of monolayer WSe$_2$ intentionally doped with vanadium atoms by means of scanning transmission electron microscopy and scanning tunneling microscopy and spectroscopy. Most of the V atoms incorporate at W sites. These V$_W$ dopants are negatively charged, which induces a localized bound state located 140 meV above the valence band maximum. The overlap of the electronic potential of two charged V$_W$ dopants generates additional in-gap states. Eventually, the negative charge may suppress the magnetic moment on the V$_W$ dopants.

Magnetism in ultra-thin films is a recent development in the field of van der Waals (vdW) layered materials. For instance, the persistence of ferromagnetism in exfoliated atomic layers has been reported only in the last few years [1, 2]. These materials present an appealing class of systems for testing the classical models for 2D magnetism, as well as for searching for exotic electronic phases and developing ultimately-thin devices [3]. Being vdW layers, they can be incorporated in stacks with other metallic, semiconducting or insulating layers [4] to create original devices, such as heterostructures showing giant tunneling magnetoresistance [5]. Moreover, through the exchange coupling at the interface [6], such vdW heterostructures can lead to a lifting of the valley degeneracy [7] in semiconducting transition metal dichalcogenides (SC-TMDs), which is one way to get a permanent valley polarization for valleytronics applications [8].

Apart from exfoliating bulk materials, a promising way to prepare magnetic vdW materials in the monolayer limit is to use direct growth techniques. Such methods are extensively used to synthetise SC-TMD compounds, with formula 1H-MX$_2$ (M=Mo or W, X=S or Se) [9]. Recent reports suggest that MnSe$_2$ [10] and VSe$_2$ [11] in the monolayer range exhibit ferromagnetism up to room temperature. However, for the former material the structure seems to change with thickness [10], whereas for the later the competition between different possible ground states may hinder the development of the ferromagnetic order [12]. An alternative approach would be to perform magnetic doping of SC-TMD by substituting 3d transition metal atoms on the M site, to create a 2D diluted magnetic semiconductors[13–20]. Among the possible candidates, vanadium is especially appealing. Its incorporation on the M sites has been demonstrated [21, 22], and a ferromagnetic behavior in moderately doped samples has been reported [22, 23]. Moreover, ab-initio calculations predict that in the ferromagnetic state there is a significant ($\sim$ 100 meV) lifting of the valley degeneracy at the K/-K points in the Brillouin zone [24], suitable for valleytronics.

In this letter, we report a study by local probe techniques of V-doped WSe$_2$ monolayers grown by molecular beam epitaxy (MBE) on epitaxial graphene on SiC. Scanning tunneling microscopy and spectroscopy (STM/STS) is an adequate technique for detecting point defects in 2D SC-TMD and for probing their local electronic structure [25–31]. With the support of additional scanning transmission electron microscopy (STEM) analysis, we identify isolated V atoms substituted on W sites (or V$_W$ dopants) in the V-doped sample, in agreement with the literature [21, 22]. Our STM/STS data reveal that the substitutional V$_W$ dopants are negatively charged, and that the resulting localized repulsive potential induces a bound state of diameter $\sim$2.2 nm, located $\sim$ 140 meV above the valence band maximum (VBM). For closely spaced V$_W$ atoms, the number and the binding energies of the bound states increase, as a consequence of the overlap of the repulsive potentials from each ionized dopant. The charging of the V$_W$ dopants results from two effects. Firstly, the V atoms should have an acceptor character [22] (as for Nb [32]), with an empty state just above the VBM in the neutral state as confirmed by density functional theory [16, 18, 21, 24, 33, 34]. Secondly the electrical contact with the graphene substrate sets the position of the Fermi level of pure WSe$_2$ well above the valence band edge [35–37], favoring a charge transfer to such acceptor state. Our result thus highlights the role of the environment in controlling the charge state of the V$_W$ dopant. This is a crucial point for magnetic doping of SC-TMD since the charge state of the 3d dopant atom significantly alters the ferromagnetic state of the system, as predicted by ab-initio calculations [14, 21, 38].

2D-WSe$_2$ flakes including a nominal amount of 3% of vanadium atoms were grown by MBE on epitaxial

graphene (EG) on SiC-Si face. All the STM/STS experiments were performed at 8.5 K [39]. From large scale STM images, we find that the monolayer TMD flakes present a large amount of individual species. They are abundant on our V-doped sample, but are mostly absent in the pristine TMD material [39]. As shown below, we ascribe them to the successful incorporation of substitutional V_W dopants in the 2D-WSe$_2$ matrix.
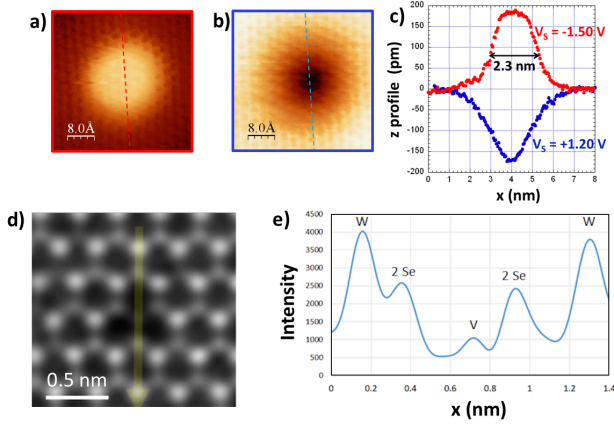

FIG. 1: STM and ADF-STEM images of individual substitutional V_W dopants incorporated in monolayer WSe$_2$. (a,b) STM images of a single V_W dopant, at sample bias V_S = -1.5V (b) and V_S = +1.2V (c). Image sizes: 4×4 nm^2. (c) Apparent height of the individual dopant, measured along the dashed lines drawn on (a) and (b) (red and blue curves respectively). (d) ADF-STEM image of a V-doped WSe$_2$ monolayer, centered on a substitutional V_W dopant. (e) Intensity profile along the vertical arrow in (d).

We first focus on the apparent STM diameter and height of one of these individual V dopants. On the images at negative and positive sample bias (Fig. 1a and Fig. 1b respectively), the atomic lattice of the TMD layer is clearly resolved, with a lattice constant of 0.33 nm. We find that the V dopant has a perfectly isotropic shape, with a sizable apparent diameter (2.30 ± 0.10 nm), i.e. $\sim$ 7 times larger than the TMD lattice constant. Moreover, the STM contrast of the dopant is reversed when the sign of the sample bias is changed, as shown in Figs. 1a and 1b (see also Ref. [39]), and on the z profiles of Fig. 1c. Eventually, since the atomic pattern of the TMD shows up even in the central disk associated to the dopant, we conclude that the surface Se atomic remains intact over the V atom. This points to an embedded dopant within the TMD layer.

We have cross-checked the presence of V_W dopants in such MBE-grown WSe$_2$ samples, by performing angular dark field (ADF) STEM measurements on a similarly V-doped sample [39]. Figure 1d is a Z-contrast (Z is the atomic number) image of that sample, centered on an apparently missing W. The intensity line profile (Fig. 1e) confirms the replacement of a W atom by a light atom.

According to the relative Z-contrast between the W sites and the central site, the substitutionally positioned light atom can be considered as a vanadium single dopant [39]. Similar STEM assessment has been proposed for the same system in Ref. [22], and STEM was also previously used to evidence V atoms substituting Mo atoms in 1L-MoS$_2$ [21].

In order to address the full electronic structure of the individual V_W dopants, we performed local tunneling spectroscopy measurements. Figure 2a presents typical $dI/dV(V)$ spectra obtained for two V_W dopants (labeled B and C in the inset). These dopants belong to a monolayer WSe$_2$ flake lying on single-layer graphene (SLG). The additional black curve in Fig. 2a is a reference spectrum recorded on the 1L-WSe$_2$ flake away from the dopants [39]. As shown in Fig. 2b, this reference spectrum, when displayed on a magnified vertical scale, defines the edges of the TMD bandgap (corresponding to the bias region with vanishing tunneling conductance). We measure a bandgap of 1.90 ± 0.06 eV, which is close to the value found for monolayer WSe$_2$ on graphitized substrate [35, 36].

Examining the $dI/dV(V)$ spectra for the two V_W dopants (red and purple curves in Fig. 2), we find that they are quantitatively very similar, confirming that the dopants have the same nature. They both exhibit several resonances within the valence band states of the TMD. One pronounced dI/dV peak, centered at at -1.16 $\pm$ 0.02 V, shows up just below the VBM. Remarkably, a second conductance peak of weaker amplitude is also found (at -1.01 $\pm$ 0.02 V as indicated by a * sign), clearly located within the TMD bandgap. We conclude that both V_W individual dopants of Fig. 2 present an in-gap state (*i.e.* a bound state), lying 0.14 ± 0.02 eV above the VBM of the 2D-TMD.

This is a robust and systematic result, associated to all tested individual V_W dopants [39]. We present in Fig. 3 a full characterization of another V_W dopant on a different TMD flake, here lying on a bilayer graphene region. The $dI/dV(V)$ spectrum associated to this dopant also indicates a bound state lying $\pm$ 0.14 eV above the VBM (see Ref. [39]). To determine its lateral extension, we performed spectroscopic measurements along a 10 nm-long line crossing the single V_W dopant (indicated by the arrow in the inset). The corresponding conductance map $dI/dV(x,V)$ is shown in Fig. 3a. The bound state, indicated by the horizontal arrow, extends over 2.2 ± 0.1 nm.

From the conductance map shown in Fig. 3a, another important result is established: Close to the V_W dopant, the STM detects spatial variations of the different band onsets (Γ peak, VBM and CBM) of the 2D-TMD. It is possible to determine such band bending quantitatively, outside the 2.2-nm wide perturbation-region centered on the dopant [39]. We show in Fig. 3b two spectra respectively measured at 2.50 nm (green curve) and 3.75
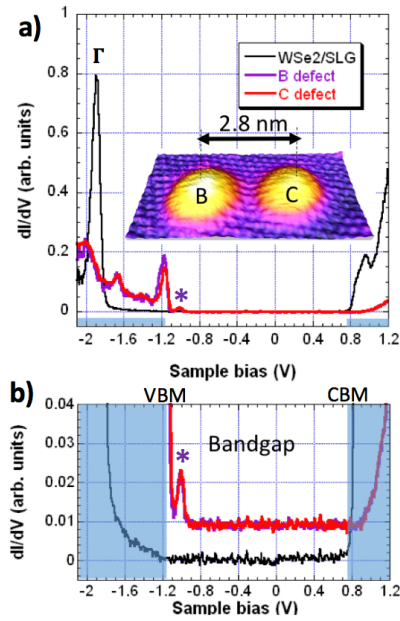
FIG. 2: STS performed at 8.5K on two neighboring V_W dopants on 1L-WSe$_2$ on single-layer graphene (SLG). (a) Local $dI/dV(V)$ spectra of the two dopants labelled B and C (respectively purple and red curves). The black curve corresponds to a spectrum performed on a nearby defect-free WSe$_2$ area, the letter Γ indicating the Γ peak, corresponding to the energy position of the valence band maximum at Γ point. The inset shows a constant current STM image of the two dopants. (b) Same as (a) with a magnified vertical scale. The white box corresponds to the TMD bandgap, VBM: Valence band maximum, CBM: Conductance band minimum. Spectra measured above the two V_W dopants are almost identical, both show a bound state (labelled *) located $\sim$0.14 eV above the VBM of the TMD. The red and purple curves are shifted vertically for clarity.

FIG. 3: STS results on a single V_W dopant on 1L-WSe$_2$ on bilayer graphene. (a) $dI/dV(x,V)$ map taken along the 10nm-long line crossing the dopant. The energy positions of the VBM, CBM and Γ peak are indicated on the map. The bound state is indicated by the white arrow. The inset shows an STM map of the area, the white line indicating the path of the tip for the map shown on (a). (b) Two $dI/dV(V)$ spectra performed at two different x positions measured from the defect center, as indicated in the inset of (a). The red curve is shifted by $\delta = +30$ mV with respect to the green curve (see text). (c) Plot of the shift δ as a function of x, evidencing a band bending by 50 meV over 2 nm.

nm (red curve) away from the dopant. The spectra look very similar, but a shift of 30 mV is necessary to align them at best. Obviously, there is an almost rigid shift of the band structure of WSe$_2$ by +30 meV when approaching the defect by 1.25 nm. We present in Fig. 3c a plot of the shift versus the tip position x with respect to the dopant. We find an upward local band bending of the TMD (by $\sim$ 50 meV over 2 nm), demonstrating that the the V_W dopant is negatively charged.

Indeed, as reported for various surfaces of semiconductors [40–42], an acceptor atom is likely to trap a net negative charge, with dramatic consequences on the local electrostatic environment. In particular, the additional negative charge gives rise to an upward local bending of the SC bands, and STM images of the impurity show a smooth and isotropic apparent-height change extending over few nm, with a strongly bias-dependent contrast [40–42]. Furthermore, the net negative charge localized at the dopant atom interacts with the holes of the valence
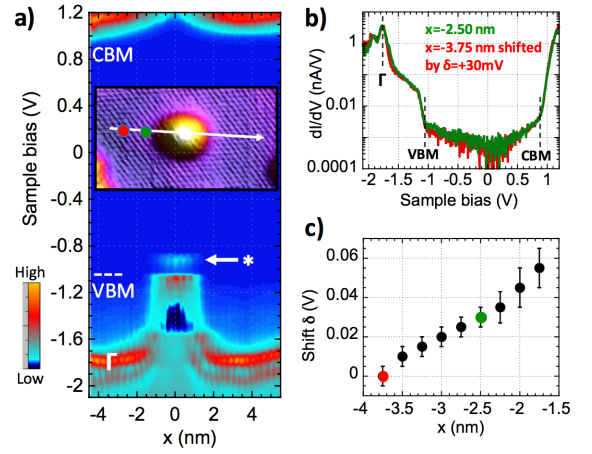
band, in a similar way to the hydrogen-like model, leading to the formation of resonances and/or bound states, i.e. states respectively lying just below or above the VBM of the SC [42–44]. In Ref. [44], the authors predict bound states centered on a negatively-charged defect with a radius in the nm range, together with a band bending region extending over several nm around the defect.

Our STM/STS findings on the individual V_W dopants, i.e. a band-bending region and a bound state above the VBM of the 2D-TMD, also reported recently for defects of uncontrolled origin [26, 30], are fully in line with this picture of a negatively charged acceptor state. Compared to W atom, V atom is lacking one d electron, and should hence behave as an acceptor when substituting W in WSe$_2$. Since EG is strongly n-doped, the substrate sets the Fermi level at least 1 eV above the VBM of bare 1L-WSe$_2$ [37]. Therefore the V-induced acceptor state is negatively charged by electronic transfer from the substrate.

To go beyond these qualitative arguments, comparison with first principle calculations is needed. Several spin-polarized calculations have been performed for V_{Mo} dopants in the cousin system 2D-MoS$_2$ [16, 18, 21, 22, 24, 33, 34, 45]. A common result in these works is a spin-polarized bound state above the VBM, reflecting the ferromagnetism predicted for the V-doped 2D-TMD. Similar findings were reported very recently for V-doped

WSe$_2$ [23]. However, in most calculations the charge state of the V atom is taken neutral, which is not the case for our configuration. At variance with the neutral case, calculation of the system with V dopants in the -1 charge state leads to zero spin polarization, suppressing magnetism in the TMD layer [21]. In Ref. [21], the computed DOS exhibits a resonance at the VBM and a (doubly) occupied state ~ 0.15 eV above the VBM, which is in line with our results.
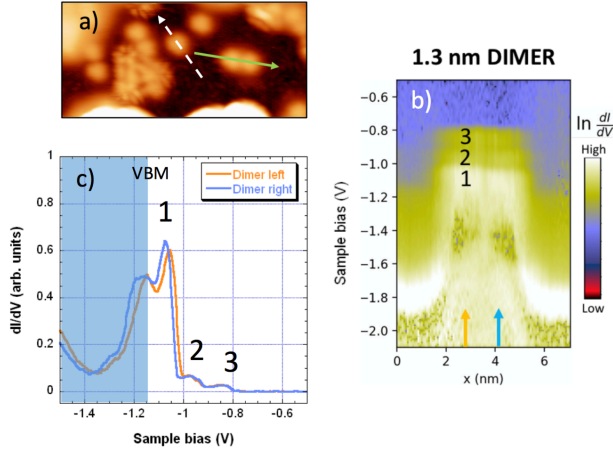

FIG. 4: Figure 4 : STS data taken on a pair of V$_W$ dopants separated by 1.3 nm. (a) Constant current STM image of the region. The 1L-WSe$_2$ flake lies on SLG. Image size: 20.0×9.5 nm^2, $V_S = -1.5$V. (b) $dI/dV(x,V)$ map, plotted in logarithmic color-scale, taken along the 7.0 nm-long line indicated by the green arrow on (a). Three conductance peaks are highlighted, labelled 1,2 and 3. (c) Individual spectra measured on the two lobes of the dimer indicated by the vertical arrows on (b).

Owing to their large apparent size, we expect a significant lateral interaction between neighboring individual V$_W$ dopants. To clarify this point, we used the STM to probe pairs of such dopants separated by short distances. As shown in Fig. 4, we collected STS data on a dimer made of two individual dopants separated by only 1.3 nm (labelled 1.3 nm dimer in the following). Such a dimer is shown in Fig. 4a, together with one individual V$_W$ dopant (located below the white arrow). We have checked in Ref. [39] that this individual dopant presents the same spectroscopic features as those reported in Figs. 2 and 3. We have then performed STS measurements along the long axis of the 1.3 nm dimer (i.e. along the green arrow in Fig. 4a). The resulting $dI/dV(x,V)$ map is shown in Fig. 4b. The spectra measured above the 1.3 nm dimer (Figs. 4b and 4c) are dramatically different from the spectra measured above isolated V$_W$ dopants: Close to the VBM, we find three in-gap peaks (labelled 1,2,3), the highest energy peak (3) lying ~ 0.3 eV above the VBM. We show in Ref. [39] a very similar result for another 1.3 nm-long dimer.

These results demonstrate that the lateral interaction

between two individual charged V$_W$ dopants is sizable when they are separated by 1.3 nm. However, we note that DFT calculations performed in a 4×4 geometry (supercell size 1.32 nm) for a neutral V$_{Mo}$ dopant in MoS$_2$ [24, 33, 34] point to a vanishing lateral interaction, since the in-gap band above the VBM is almost flat. We believe that the long range interaction, which shows up in Figs. 4b and 4c, occurs due to the fact that the V$_W$ dopants are negatively charged in our sample. Simple electrostatic considerations [44] qualitatively explain the results that we obtain for the 1.3 nm dimer. In such a configuration, the electrostatic potentials of the closely spaced dopants overlap. Hence the potential well for the holes is wider and deeper for the dimer than for the individual dopant. As a consequence, additional and more strongly bound hydrogenic-like in-gap states can show up [44], and we ascribe the peaks labelled 1,2,3 in the spectra of Fig. 4 to such electrostatically-induced in-gap states. The observation of even more strongly bound states in larger clusters of V$_W$ dopants (see Ref. [39]) clearly supports the electrostatic origin of the V-induced bound states in our system.

In summary, we report here a thorough experimental study of the atomic and electronic structure of individual V dopants incorporated in monolayer WSe$_2$. Based on STM/STS techniques complemented by ADF-STEM measurements, our work shows that the V atoms are substitutional dopants at W sites of the 2D-TMD, and that they are negatively charged by a charge transfer from the n-doped graphene substrate. This net localized charge gives rise to a bound state with a diameter of around 2.2 nm, located ~ 140 meV above the valence band maximum of WSe$_2$. Following recent DFT calculation [14, 21, 38], this negative charge state of the V$_W$ dopant should impact the magnetic properties of the system, and possibly hinder any ferromagnetism in the 2D TMD layer. An appealing perspective would be to manipulate the charge state of the dopants by using an electrostatic backgate, in order to tune the magnetism of the 2D crystal.

---

* electronic address: `pierre.mallet@neel.cnrs.fr`

REFERENCES

[1] C. Gong, L. Li, Z. Li, H. Ji, A. Stern, Y. Wia, T. Cao, W. Bao, C. Wang, Y. Wang et al, Nature **546**, 265 (2017)

[2] B. Huang, G. Clark, E. Navarro-Moratalla, D.R. Klein, E. Cheng, K.L. Seyler, D. Zhong, E. Schmidgall, M.A. McGuire, D.H. Cobden et al, Nature **546**, 270 (2017)

[3] K. S. Burch, D. Mandrus and J. G. Park, Nature **563**, 47 (2018)

[4] K. S. Novoselov, A. Mishchenko, A. Carvalho and A.H. Castro Neto, Science **353**, 6298 (2016); C. Gong and X. Zhang, Science **363**, 4450 (2019)

[5] T. Song, X. Cai, M.W-Y Tu, X. Zhang, B. Huang, N.P. Wilson, K.L. Seyler, L. Zhu, T. Taniguchi, K. Watanabe et al, Science **360**, 1214 (2018); D.R. Klein, D. MacNeill, J.L. Lado, D. Soriano, E. Navarro-Moratalla, K. Watanabe, T. Taniguchi, S. Manni, P. Canfield, J. Fernández-Rossier et al., Science **360**, 1218 (2018)

[6] C. Zhao, T. Norden, P. Zhang, P. Zhao, Y. Cheng, F. Sun, J.P. Parry, P. Taheri, J. Wang, Y. Yang et al., Nat. Nanotech. **12**, 757 (2017)

[7] D Zhong, K.L. Seyler, X. Linpeng, R. Cheng, N. Sivadas, B. Huang, E. Schmidgall, T. Taniguchi, K. Watanabe, M.A. McGuire et al., Sci. Adv. **3**, e1603113 (2017)

[8] S.A. Vitale, D. Nezich, J.O. Varghese, P. Kim, N. Gedik, P. Jarillo-Herrero, D. Xiao and M. Rothschild, Small **14**, 1801483 (2018)

[9] W. Choi, N. Choudhary, G.H. Han, J. Park, D. Akinwande and Y.H. Lee, Materials Today **20**, 116 (2017)

[10] D.J. O'Hara, T. Zhu, A.H. Trout, A.S. Ahmed, Y.K. Luo, C.H. Lee, M.R. Brenner, S. Rajan, J.A. Gupta, D.W. McComb et al, Nano Lett. **18**, 3125 (2018)

[11] M. Bonilla, S. Kolekar, Y. Ma, H.C. Diaz, V. Kalappattil, R. Das, T. Eggers, H.R. Guttierrez, M.H. Phan and M. Batzill, Nat. Nanotech. **13**, 289 (2018)

[12] J. Feng, D. Biswas, A. Rajan, M.D. Watson, F. Mazzola, O.C. Clark, K. Underwood, I. Markovic, M. McLaren, A. Hunter et al, Nano Lett. **18**, 4493 (2018)

[13] Y.C. Cheng, Z.Y. Zhu, W.B. Mi, Z.B. Guo and U. Schwingenschlögl, Phys. Rev. B **87**, 100401 (R) (2013)

[14] R. Mishra, W. Zhou, S.J. Pennycook, S.T. Pantelides and J.-C. Idrobo, Phys. Rev. B **88**, 144409 (2013)

[15] A. Ramasubramaniam and D. Naveh, Phys. Rev. B **87**, 195201 (2013)

[16] X.L. Fan, Y.R. An and W.J. Guo, Nanoscale Research Lett. **11**, 154 (2016)

[17] L.Y. Xie and J.M. Zhang, Superlattices and Microstructures **98**, 148 (2016)

[18] M. Wu, X. Yao, Y. Hao, H. Dong, Y. Cheng, H. Liu, F. Lu, W. Wang, K. Cho and W.-H. Wang, Phys. Lett. A **382**, 111 (2018)

[19] A.N. Andriotis and M. Menon, Phys. Rev. B **90**, 125304 (2014)

[20] K. Zhang, S. Feng, J. Wang, A. Azcati, N. Lu, R. Addou, N. Wang, C. Zhou, J. Lerach, V. Bojan et al., Nano Lett. **15**, 6586 (2015)

[21] A. Robertson, Y.-C. Lin, S. Wang, H. Sawada, C.S. Allen, Q. Chen, S. Lee, G.-D. Lee, J. Lee, S. Han et al., ACS Nano **10**, 10227(2016)

[22] S.J. Yun, D.L. Duong, M.H. Doan, K. Singh, T.L. Phan, W. Choi, Y.-M. Kim and Y.H. Lee, arXiv:1806.06479 (2018)

[23] D.L. Duong, S.J. Yun, Y. Kim, S.-G. Kim and Y.H. Lee, Appl. Phys. Lett. **115**, 242406 (2019)

[24] N. Singh and U. Schwingenschlögl, Adv. Mater. **29**, 1600970 (2017)

[25] B. Schuler, D.Y. Qui, S. Refaely-Abramson, C. Kastl, C.T. Chen, S. Barja, R.J. Koch, D.F. Ogletree, S. Aloni, A.M. Schwartzberg et al., Phys. Rev. Lett. **123**, 076801(2019)

[26] B. Schuler, J.-H. Lee, C. Kastl, K.A. Cochrane, C.T. Chen, S. Refaely-Abramson, S. Yuan, E. van Veen, R. Roldán, N.J. Borys et al., ACS Nano **13**, 10520 (2019)

[27] S. Barja, S.Refaely-Abramson, B. Schuler, D.Y. Qiu, A. Pulkin, S. Wickenburg, H. Ryu, M.M. Ugeda, C. Kastl, C. Chen et al., Nat. Commun. **10**, 3382 (2019)

[28] Y.C. Lin, B. Jariwala, B.M. Bersch, K. Xu, Y. Nie, B. Wang, S.M. Eichfeld, X. Zhang, T.H. Choudhury, Y. Pan et al., ACS Nano **12**, 965 (2018)

[29] S. Zhang, C.-G. Wang, M.-Y. Li, D. Huang, L.-J. Li, W. Ji and S. Wu., Phys. Rev. Lett. **119**, 046101 (2017)

[30] T. Le Quang, K. Nogajewski, M. Potemski, M.T. Dau, M. Jamet, P. Mallet and J.-Y. Veuillen, 2D Mater. **5**, 035034 (2018)

[31] C. Zhang, C. Wang, F. Yang, J.-K. Huang, L.-J. Li, W. Yao, W. Ji and C.-K. Shih, ACS Nano **13**, 1592 (2019)

[32] R. Mukherjee, H. J. Chuang, M. R. Koehler, N. Combs, A. Patchen, Z. X. Zhou, and D. Mandrus, Phys. Rev. Appl. **7**, 1034011 (2017)

[33] Y. Miao, Y. Li, Q. Fang, Y. Huang, Y. Sun, K. Xu, F. Ma and P.K. Chu, Applied Surface Science **428**, 226 (2018)

[34] S. Mekonnen and P. Singh, Int. J. Mod. Phys. B **32**, 1850231 (2018)

[35] Y. Zhang, M.M. Ugeda , C. Jin, S.-F. Shi, A.J. Bradley, A. Martín-Recio, H. Ryu, J. Kim, S. Tang, Y. Kim et al., Nano Lett. **16**, 2485 (2016)

[36] C. Zhang, Y. Chen, A. Johnson, M.-Y. Li, L.-J. Li, P.C. Mende, R.M. Feenstra and C.-K. Shih, Nano Lett. **15**, 6494 (2015)

[37] T. Le Quang, V. Cherkez, K. Nogajewski, M. Potemski, M.T. Dau, M. Jamet, P. Mallet and J.-Y. Veuilen, 2D Mater. **4**, 035019 (2017)

[38] X. Lin and J. Ni, J. Appl. Phys. **116**, 044311 (2014)

[39] See supplemental material at http:// for details on sample preparation and experimental methods, and additional STM/STS and STEM data. Supplemental material includes Refs. [46-58].

[40] J.A. Stroscio, R.M. Feenstra and A.P. Fein, Phys. Rev. Lett. **58**, 1668 (1987)

[41] A.M. Yakunin, A.Y. Silov, P.M. Koenraad, J.H. Wolter, W. Van Roy, J. De Boeck, J.-M. Tang and M.E. Flatté, Phys. Rev. Lett. **92**, 216806 (2004)

[42] Z. Qiu, H. Fang, A. Carvalho, A.S. Rodin, Y. Liu, S.J.R. Tan, M. Telychko, P. Lv, J. Su, Y. Wang et al., Nano Lett. **17**, 6935 (2017)

[43] N.W. Ashcroft and N.D. Mermin, Solid State Physics, Saunders College Publishing, Harcourt College Publishers (1976)

[44] M. Aghajanian, A.A. Mostofi and J. Lischner, Sci. Rep. **8**, 13611 (2018)

[45] C. Gonzalez, B. Biel and Y.J. Dappe, Nanotechnology **27**, 105702 (2016)

[46] P. Mallet, F. Varchon, C. Naud, L. Magaud, C. Berger and J.-Y. Veuillen, Phys. Rev. B **76**, 041403(R) (2007)

[47] I. Forbeaux, J.M. Themlin and J.M. Debever, Phys. Rev. B **58**, 16396 (1998)

[48] C. Berger, Z. Song, X. Li, X. Wu, N. Brown, C. Naud, D.

Mayou, T. Li, J. Hass, A.N. Marchenkov et al., Science **312**, 1191 (2006)

[49] J. He, N. Kumar, M.Z. Bellus, H.-Y. Chiu, D. He, Y. Wang and H. Zhao, Nat. Commun. **5**, 5622 (2014)

[50] I. Horcas, R. Fernández, J.M. Gómez-Rodríguez, J. Colchero, J. Gómez-Herrero and A.M. Baro, Rev. Sci. Instrum. **78**, 013705 (2007)

[51] G.M. Rutter, N.P. Guisinger, J.N. Crain, E.A.A. Jarvis, M.D. Stiles, T. Li, P.N. First and J.A. Stroscio, Phys. Rev. B **76**, 235416 (2007)

[52] C. Zhang, Y. Chen, J.-K. Huang, X. Wu, L.-J. Li, W. Yao, J. Tersoff and C.-K. Shih, Nat. Commun. **7**, 10349 (2016)

[53] M.M. Ugeda, A.J. Bradley, S.-F. Shi, F.H. da Jornada, Y. Zhang, D.Y. Qiu, W. Ruan, S.-K. Mo, Z. Hussain, Z.-X. Shen et al., Nat. Mater. **13**, 1091 (2014)

[54] P. Lauffer, K.V. Emtsev, R. Graupner, Th. Seyller, L. Ley, S.A. Reshanov and H.B. Weber, Phys. Rev. B **77**, 155426 (2008)

[55] I. Brihuega, P. Mallet, C. Bena, S. Bose, C. Michaelis, L. Vitali, F. Varchon, L. Magaud, K. Kern and J.Y. Veuillen, Phys. Rev. Lett. **101**, 206802 (2008)

[56] K. Teichmann, M. Wenderoth, S. Loth, R.G. Ulbrich, J.K. Garleff, A.P. Wijnheijnmer and P.M. Koenraad, Phys. Rev. Lett. **101**, 076103 (2008)

[57] H. Zheng, J. Kröger and R. Berndt, Phys. Rev. Lett. **108**, 076801 (2012)

[58] Y. Liu, P. Stradins and S.-Y. Wei, Sci. Adv. **2**, e1600069 (2016)